Published in final edited form as:

Invest Radiol. 2015 November ; 50(11): 749–756. doi:10.1097/RLI.0000000000000179.

Respiratory Motion-Resolved Compressed Sensing Reconstruction of Free-Breathing Radial Acquisition for Dynamic Liver MRI

Hersh Chandarana, MD[1,2], **Li Feng, PhD**[1,2], **Justin Ream, MD**[2], **Annie Wang, MD**[2], **James S Babb, PhD**[1,2], **Kai Tobias Block, PhD**[1,2], **Daniel K Sodickson, MD, PhD**[1,2], and **Ricardo Otazo, PhD**[1,2]

[1]Center for Advanced Imaging Innovation and Research (CAI[2]R), New York University School of Medicine, New York, NY USA

[2]Bernard and Irene Schwartz Center for Biomedical Imaging, Department of Radiology, New York University School of Medicine, New York, NY USA

Abstract

Purpose—Demonstrate feasibility of free-breathing radial acquisition with respiratory motion-resolved compressed sensing (CS) reconstruction (XD-GRASP) for multiphase dynamic Gd-EOB-DTPA enhanced liver imaging, and compare image quality to CS reconstruction with respiratory motion-averaging (GRASP) and prior conventional breath-held Cartesian-sampled datasets (BH-VIBE) in same patients.

Subjects and Methods—In this HIPAA-compliant prospective study, 16 subjects underwent free-breathing continuous radial acquisition during Gd-EOB-DTPA injection, and had prior BH-VIBE exam available. Acquired data were reconstructed using motion-averaging GRASP approach, in which consecutive 84-spokes were grouped in each contrast-enhanced phase for a temporal resolution of ~14 seconds. Additionally, respiratory motion-resolved reconstruction was performed from the same k-space data, by sorting each contrast-enhanced phase into multiple respiratory motion states using compressed sensing algorithm named XD-GRASP, which exploits sparsity along both the contrast-enhancement and respiratory-state dimensions.

Contrast-enhanced dynamic multi-phase XD-GRASP, GRASP, and BH-VIBE images were anonymized, pooled together in a random order and presented to two board-certified radiologists for independent evaluation of image quality, with higher score indicating more optimal exam.

Results—XD-GRASP reconstructions had significantly (all $p<0.05$) higher overall image quality scores compared to GRASP for early arterial (Reader 1: **4.3 ± 0.6 vs. 3.31 ± 0.6** ; Reader 2: **3.81 ± 0.8 vs. 3.38 ± 0.9**) and late arterial (Reader 1: **4.5 ± 0.6 vs. 3.63 ± 0.6**; Reader 2: **3.56 ± 0.5 vs. 2.88 ± 0.7**) phases of enhancement for both readers. XD-GRASP also had higher overall image quality score in portal venous phase which was significant for Reader 1 (**4.44 ± 0.5 vs. 3.75 ± 0.8; p=0.002**). In addition, XD-GRASP had higher overall image quality score compared to BH-VIBE

Corresponding author: Hersh Chandarana, MD., New York University Langone Medical Center, Department of Radiology, 660 First Avenue, New York, NY 10016, Phone: 212-263-0232, Fax: 212-263-6634, hersh.chandarana@nyumc.org.

for early (Reader 1: **4.3±0.6 vs. 3.88±0.6**; Reader 2: **3.81±0.8 vs. 3.50±1.0**) and late (Reader 1: **4.5±0.6 vs. 3.44±0.6**; Reader 2: **3.56±0.5 vs. 2.94±0.9**) arterial phases.

Conclusion—Free-breathing motion-resolved XD-GRASP reconstructions provide diagnostic high-quality multiphase images in patients undergoing Gd-EOB-DTPA-enhanced liver exam.

Introduction

Hepatobiliary contrast agent Gd-EOB-DTPA enhanced liver imaging has been shown to improve detection of small metastasis, discriminate focal nodular hyperplasia (FNH) from adenoma [1–3], detect small hepatocellular carcinomas (HCC), discriminate regenerative/dysplastic nodules and other pseudolesions from hepatocellular carcinomas (HCC), and potentially discriminate HCC of differing aggressiveness [4–11].

Assessment of arterial enhancement, irrespective of the contrast (extracellular or hepatobiliary) agent, is essential in detection and characterization of liver lesions. Optimal timing of the arterial phase, with highest contrast between the lesion and background liver parenchyma, is desired. This is more reliably achieved with timing run or fluoroscopic triggering compared to a fixed timing delay [12, 13]. Various studies have suggested that acquisition of multiple arterial phases can improve the detection of enhancement in liver lesions [14, 15]. Many groups perform dual arterial phase acquisition in one breath-hold to improve the conspicuity of arterial enhancement in small lesions [16]. However, the need to acquire data within a breath-hold requires a balance between temporal resolution, spatial resolution, and volumetric coverage. These concerns are accentuated with use of the hepatobiliary contrast agent Gd-EOB-DTPA due to lower contrast dose, injected volume, and rate compared to the extracellular contrast agents. Recently published reports of transient dyspnea associated with this contrast agent have amplified these concerns for detection of arterial enhancement in small hepatic lesions [17–19].

A recently introduced free-breathing imaging technique combining compressed sensing (CS) and parallel imaging with golden-angle radial sampling (GRASP- Golden-angle RAdial Sparse Parallel imaging) may help overcome many of the limitations listed above [20, 21]. Radial acquisition has lower sensitivity to respiratory motion when compared to conventional Cartesian sampling schemes due to the motion averaging effect from the repeated sampling of k-space center [22, 23]. Moreover, golden-angle radial sampling allows continuous data acquisition and retrospective reconstruction with a flexible temporal resolution by grouping a specific number of successive spokes together, so that appropriate phases of enhancement can be generated [24]. A preliminary study has shown that GRASP produces good image quality in the venous phase, and diagnostic but relatively lower image quality in the arterial phase as compared to the conventional breath-held Cartesian acquisition in healthy subjects undergoing imaging with an extracellular contrast agent [20]. Further improvement of image quality of the arterial phases in GRASP is desirable.

The oversampling of k-space center in radial imaging provides additional opportunity for self-navigation, which can be exploited to minimize the respiratory motion blurring effects. Instead of averaging motion, as performed in GRASP reconstruction, an extra respiratory motion dimension can be reconstructed from the continuously acquired k-space data, by

sorting each contrast-enhanced phase into multiple respiratory motion states, spanning from end-inspiration to end-expiration (Figure 1). A compressed sensing algorithm that exploits sparsity along both the contrast-enhancement dimension and the respiratory-state dimension [25] can be subsequently employed to reconstruct the motion-resolved undersampled dataset. This image reconstruction framework, called XD-GRASP (eXtra-Dimensional Golden-Angle RAdial Sparse Parallel), generates multi-dimensional dynamic image sets with resolved respiratory motion in each contrast-enhanced dynamic phase.

The aim of this study is to demonstrate feasibility of free-breathing radial acquisition with respiratory motion-resolved compressed sensing (CS) reconstruction (XD-GRASP) for multiphase dynamic Gd-EOB-DTPA enhanced liver imaging, and compare image quality to CS reconstruction with respiratory motion-averaging (GRASP) and also prior conventional breath-held Cartesian-sampled datasets (BH-VIBE) in same patients.

Subjects and Methods

In this HIPAA compliant IRB approved prospective study, patients scheduled for clinically indicated Gd-EOB-DTPA enhanced liver MRI from January 2014 to September 2014 were recruited to undergo free-breathing dynamic imaging of the liver with continuous golden-angle radial acquisition instead of conventional breath-hold Cartesian acquisition. The inclusion criteria were as follows: (1) Patients scheduled on a scanner equipped to perform radial acquisition either for evaluation of liver cirrhosis or for evaluation of known or suspected focal liver lesions; and (2) Prior conventional Cartesian breath-hold MRI. Informed consent was obtained for all patients.

Patients

34 patients agreed to participate in the study. In 16 of these patients, prior conventional Cartesian breath-hold exam with Gd-EOB-DTPA performed at the same field strength was available, and these patients constituted our study cohort. 9 females (mean age 48.5 ± 12.5 years, range 33.2–70.4 years) and 7 males (mean age 56.1 ± 6.1 years, range 47.9–64.6 years) were included in our study. 10 patients had an established diagnosis of cirrhosis and were being scanned for routine surveillance. 6 non-cirrhotic patients were imaged; 5 patients were being scanned for follow-up of benign hepatic lesions; and 1 patient was scanned for surveillance status post orthotopic liver transplant.

MR Imaging

MR imaging was performed on a 1.5-T whole-body clinical scanner (Siemens MAGNETOM Avanto, Erlangen, Germany) equipped with body and spine phased-array coils. All subjects underwent axial breath-hold T1 gradient echo (GRE) in and out of phase, axial breath-hold fat suppressed T2 turbo spin echo (TSE), axial DWI in free-breathing, and coronal breath-hold T2 HASTE (Half Fourier Acquisition Single shot Turbo spin Echo) acquisitions prior to contrast administration. Subsequently, a stack-of-stars 3D Radial GRE sequence with golden-angle ordering scheme was employed during free-breathing while intravenous contrast was injected. A total of 1904 radial spokes were continuously acquired in 318–340 seconds with the following parameters: slice thickness = 3 mm, flip angle = 12°,

FOV = 385 × 385 mm^2, matrix size= 256 × 256, spatial resolution = 1.5×1.5×3 mm^3, TR/TE = 3.97–4.29 ms / 1.71 ms, and bandwidth = 450Hz/pixel. 72 partitions were acquired (interpolated) with 6/8 partial-Fourier performed along the slice-encoding dimension. Intravenous injection of 10 mL Gd-EOB-DTPA (Eovist, Bayer HealthCare) was initiated 20 seconds after commencement of scanning via a power injector at a rate of 1 mL/s, followed by a 20 mL saline flush also at a rate of 1 mL/s. No timing run or bolus tracking was performed.

GRASP Reconstruction—Image reconstruction was performed off-line as previously described [21] using temporal finite differences (to minimize the temporal total variation) as a sparsifying transform. Compressed sensing and parallel imaging were combined to exploit joint multicoil sparsity. 84 spokes were grouped together in each dynamic frame for a temporal resolution of ~14 seconds. The reconstruction was implemented in MATLAB (The MathWorks, MA) using an iterative non-linear conjugate gradient algorithm.

XD-GRASP Reconstruction—In order to detect the respiratory motion signal, a one-dimensional Fourier transform along the partition dimension was first performed on the central k-space points at each acquisition angle. This produced a projection profile of the entire volume along that dimension corresponding to acquisition of all partitions at a given spoke angle in the stack-of-stars trajectory. The respiratory motion signal was estimated by concatenating the projection profiles from all coils into a large two dimensional matrix, followed by principal component analysis (PCA) along the z+coil dimension, in order to determine the most common signal variation mode among all the coil elements. The principal component with the highest peak in the frequency range of 0.1–0.5Hz was automatically selected to represent respiratory motion. Contrast-enhancement was suppressed from the respiratory motion signal by subtracting the envelope, which was estimated using a spline data fitting procedure.

XD-GRASP reconstruction was framed as an extension of the GRASP reconstruction algorithm, with enforcement of an additional sparsity constraint along the respiratory-state dimension. The optimization problem is formulated as:

$$x=\min_{x}\|F\cdot C\cdot x-y\|_2^2+\lambda_1\|S_1\cdot x\|_1+\lambda_2\|S_2\cdot x\|_1 \quad [1]$$

where F is the non-uniform fast Fourier transform (NUFFT) [26] operator defined in the radial sampling pattern, $C = [C_1,C_2\ldots C_n]$ are n-element coil sensitivity maps,×is the dynamic image to be reconstructed and $y = [y_1,y_2\ldots y_n]$ are the multicoil radial k-space data sorted according to the new dimensions. S_1 is the sparsifying transform applied in the newly isolated contrast-enhancement dimension and S_2 is the sparsifying transform applied along the extra respiratory-phase dimension. In this work, temporal finite difference transforms were employed in both S_1 and S_2, but with different weights λ_1 and λ_2 tailored to the sparsity along each dynamic dimension.

For consistency, 84 consecutive spokes were used for each contrast-enhancement phase, both for GRASP – in which the single dynamic dimension represented contrast enhancement perturbed by motion – and for XD-GRASP, in which each isolated contrast-enhancement

phase was sorted into 4 respiratory motion states, spanning from end-inspiration to end-expiration. For XD-GRASP, the reconstructed end-expiratory state (which matches the breath-hold acquisition) was utilized for qualitative image analysis.

Prior Cartesian Exam Details—All patients had a prior scan with standard breath-hold Cartesian pre-and post-contrast acquisition performed on the same 1.5-T clinical system (Siemens MAGNETOM Avanto, Erlangen, Germany). Average time interval between the current study and this prior conventional breath-hold examination was 406.9 +/− 265.3 days, with a range of 133–923 days. MELD scores for the 10 cirrhotic subjects prior to the conventional exam ranged from 6 to 14 with average of 9.2. There MELD scores prior to the current XD-GRASP exam were not significantly different (p=0.26) and ranged from 7 to 18 with average of 9.8. Patients underwent 1 pre-contrast and 4 post-contrast axial T1-weighted 3D GRE acquisitions, including two arterial phases in one breath-hold, followed by breath-held portal venous and late dynamic phase acquisitions. Bolus tracking with fluoroscopic triggering was used to obtain optimal arterial phase timing delay. Imaging parameters were as follows: slice thickness = 2.0–3.4 mm, flip angle = 12°, FOV = 325–425 × 178–297 mm^2, in plane spatial resolution (interpolated)= 1.3–1.7 × 1.3–1.7 mm^2. 10 mL Gd-EOB-DTPA (Eovist, Bayer HealthCare) was injected intravenously via a power injector at a rate of 1 mL/s, followed by a 20 mL saline flush also at a rate of 1 mL/s.

Image Analysis—For all patients, non-contrast, early arterial, late arterial and portal venous enhancement phase images were selected from both GRASP and XD-GRASP reconstructions by an experienced radiologist who did not perform image analysis. These reconstructions and the prior breath-hold multiphase acquisitions were stripped of patient and acquisition parameter details. Images were pooled together in a random order and presented to two board-certified radiologists (_,_) with 2 and 3 years of abdominal MRI experience, respectively, for independent evaluation of the image quality. Prior to formal image quality evaluation readers underwent a short training session.

Both readers first identified the enhancement pattern of the liver as non-contrast, early arterial, late arterial or portal venous for each dataset. Subsequently, the following metrics of image quality were scored using a 5 point scale (1–5), with the highest score indicating the most desirable exam (Table 1): overall image quality (IQ), liver edge sharpness, hepatic vessel clarity, and streak artifact.

In a separate sitting, 2 months after the initial image quality evaluation, both readers also independently assessed for presence of enhancing lesions greater than 0.5 cm in size. Multiphase (pre-contrast, early arterial, late arterial, and portal venous phase) GRASP and multiphase XD-GRASP reconstructions for each of the 16 subjects, for a total of 32 multiphase datasets, were randomized and presented to the two readers. If a lesion was identified, the readers noted the location of the lesion and scored the lesion conspicuity as well as the lesion edge sharpness on the same 5-point scale on multi-phase contrast enhanced acquisitions (Table 1).

Statistical Analysis

Image quality parameters for each subject were recorded by each reader for each acquisition. This was used to compute mean and standard deviation scores for each parameter of image quality for each phase of enhancement stratified by reader. A paired sample Wilcoxon signed rank test was performed to compare acquisitions in terms of the quality scores.

The mean and standard deviation (SD) of lesion conspicuity and lesion sharpness scores from each reader for GRASP and XD-GRASP data sets were noted. GRASP and XD-GRASP were compared accounting for the natural pairing of the data (i.e. each lesion could be assessed with both reconstructions). Within-lesion differences in conspicuity and sharpness from each reader were computed as the score for XD-GRASP minus the score for GRASP. Wilcoxon signed rank and was used to compare the XD-GRASP and GRASP in terms of lesion conspicuity and sharpness. To account for within-subject correlations, scores from multiple lesions was averaged as a single score. All statistical tests were conducted at the two-sided 5% significance level using SAS 9.3 (SAS Institute, Cary, NC).

Results

Overall Image Quality

XD-GRASP had higher overall image quality scores compared to GRASP for all phases of enhancement (Table 2A) for both readers. This was significant (all $p < 0.05$) for all phases of enhancement except for non-contrast acquisition for reader 1 and for portal venous phase for reader 2 (Table 2B). In addition, XD-GRASP had higher overall image quality scores compared to breath-held early and later arterial phase VIBE acquisitions for both readers. There were no significant differences in overall image quality scores for non-contrast and portal venous phases between XD-GRASP and BH-VIBE (Figure 2 and Figure 3).

Hepatic Vessel Clarity

XD-GRASP had significantly higher scores for hepatic vessel clarity compared to GRASP for the early arterial, late arterial and portal venous phases of enhancement for reader 1. The scores of XD-GRASP were also higher than GRASP for reader 2 for the early and late arterial phases but this did not reach statistical significance (Table 3A & 3B).

Liver Edge Sharpness

Scores for liver edge sharpness were significantly higher with XD-GRASP compared to GRASP for reader 1 in the early arterial, late arterial and portal venous phases. For reader 2, XD-GRASP also received higher scores for all phases of enhancement except portal venous phase, but this did not reach statistical significance (Table 4A & 4B). The liver edge sharpness scores of XD-GRASP were higher than those of BH-VIBE for the early arterial and late arterial phases of enhancement for both the readers.

Streak artifact

XD-GRASP showed reduced streak artifact and higher scores as compared to GRASP for all phases of enhancement for both readers which was significant for reader 1 for all phases of enhancement (all $p<0.05$) but was not significant for reader 2 (Table 5).

Lesion Evaluation

Reader 1 identified the same 12 enhancing lesions larger than 0.5 cm on XD-GRASP and GRASP. Reader 2 identified 11 enhancing lesions on XD-GRASP and 10 enhancing lesions on GRASP (Figure 4).

For both readers XD-GRASP had higher scores compared to GRASP for lesion conspicuity (**Reader 1**: 4.5 ± 0.67 versus 4.17 ± 1.03; **Reader 2**: 4.45 ± 0.52 versus 3.70 ± 1.16) and lesion edge sharpness (**Reader 1**: 3.92 ± 0.67 versus 2.92 ± 1.16; **Reader 2**: 4.27 ± 0.47 versus 3.50 ± 1.08). However, these differences did not reach statistical significance (all $p \geq 0.06$).

Discussion

Gd-EOB-DTPA exhibits high T_1 relaxivity in the liver, and shows peak enhancement in the normal liver approximately 20 minutes after injection on T_1-weighted MR images [27–29]. This property of the Gd-EOB-DTPA can improve diagnosis of small hepatocellular carcinoma and metastases, and can also improve the characterization of liver lesions. However, some of the drawbacks associated with its routine use include a concern about reduced vessel and parenchymal enhancement due to lower contrast dose and volume [30], and also a concern with regards to image quality of the arterial phases due to respiratory motion [18].

Radial acquisition has improved motion robustness and hence it is a promising approach for free-breathing abdominal imaging [31]. A recent study in pediatric patients showed improved image quality and lesion conspicuity of the post-contrast radial acquisition compared to Cartesian acquisition [32]. However, in another study the inherent motion averaging effects in the arterial phase GRASP reconstruction resulted in relatively lower image quality with residual blurring when compared to conventional multiphase contrast enhanced examination in healthy subjects [20]. To solve the problem of respiratory motion, we exploited the self-navigation properties of radial sampling and utilized the fact that the respiratory motion is highly correlated and therefore compressible. XD-GRASP does not rely upon any particular motion model, and it resolves respiratory motion into distinct motion-states. Thus, it provides the ability to visualize images at different respiratory motion states from end-inspiration to end-expiration.

Our results are promising as they not only demonstrate improved image quality with XD-GRASP reconstruction compared to GRASP, but also demonstrate that the end-expiratory phase in XD-GRASP reconstruction outperforms the conventional arterial breath-hold Cartesian acquisition also performed in end-expiration. These results have the potential to improve post-contrast imaging in patients undergoing MR imaging of the liver with Gd-EOB-DTPA, and to overcome many of the limitations associated with Gd-EOB-DTPA enhanced liver MR examination. However, other approaches such as advance parallel imaging can also be used to shorten the breath-hold duration thus improving image quality in patients with limited breath-hold capacity [33, 34]. Larger studies with head-to-head comparison between different approaches will be required to identify subset of patients that

would benefit from free-breathing XD-GRASP acquisition over shortened breath-held techniques.

Following the introduction of XD-GRASP, similar approaches have been proposed using different k-space trajectories such as Cartesian trajectories with butterfly navigators [35]. The use of Cartesian trajectories may enable faster reconstruction of the high dimensional dataset, but at the expense of having different undersampling patterns for each respiratory motion state. By contrast, golden-angle radial sampling results in more uniform sampling patterns for each respiratory motion state. Moreover, Cartesian sampling also loses the motion robustness that is inherent to radial sampling.

There are several limitations of our study. Firstly, we used only reconstructions in end-expiratory phase for image evaluation, and excluded data reconstructed in other respiratory phases. This is inefficient, as large quantities of potentially useful data are discarded in this approach. Elastic registration algorithms can hopefully overcome this loss of data by combining images acquired in multiple motion states. Secondly, only a small number of patients were included in our study. However, in this prospective study we included patients who had prior conventional breath-hold imaging with the same contrast agent (Gd-EOB-DTPA) and on the same field strength (1.5 T) system. There was a relatively long delay between the conventional exam and the current radial GRASP/XD-GRASP exam. Although there were no significant changes in MELD scores obtained prior to the BH-VIBE and XD-GRASP exams, it is possible that the patients' health and breath-hold capacity could have changed during this time period. However, it was not practical logistically to image same patients twice with 2 full doses of contrast injections in rapid succession for research purposes. Subjective evaluation of image quality introduces inter-reader variability as evident by differences in absolute scores of image quality provided by the two readers. However, for both readers similar trends of higher image quality scores for XD-GRASP compared to GRASP were noted..

In conclusion, this study has shown that XD-GRASP is able to resolve respiratory motion in the radial acquisition, and thus guide compressed sensing reconstruction of multiphase dynamic data for liver imaging with image quality superior to that obtained with standard GRASP reconstructions. Furthermore, the arterial phases XD-GRASP reconstructions from free-breathing continuous radial acquisition achieved higher overall image quality compared to the conventional breath-hold arterial phase Cartesian acquisitions. The proposed XD-GRASP approach has the potential to improve contrast-enhanced dynamic liver imaging with continuous data acquisition and retrospective motion-resolved reconstruction.

Acknowledgement

The Center for Advanced Imaging Innovation and Research (CAI^{2}R, www.cai2r.net) at New York University School of Medicine is supported by NIH/NIBIB grant number P41 EB017183.

References

1. Hammerstingl R, Huppertz A, Breuer J, et al. Diagnostic efficacy of gadoxetic acid (Primovist)-enhanced MRI and spiral CT for a therapeutic strategy: comparison with intraoperative and

histopathologic findings in focal liver lesions. European radiology. 2008; 18:457–467. [PubMed: 18058107]

2. Scharitzer M, Ba-Ssalamah A, Ringl H, et al. Preoperative evaluation of colorectal liver metastases: comparison between gadoxetic acid-enhanced 3.0-T MRI and contrast-enhanced MDCT with histopathological correlation. European radiology. 2013; 23:2187–2196. [PubMed: 23519439]
3. Zech CJ, Grazioli L, Breuer J, Reiser MF, Schoenberg SO. Diagnostic performance and description of morphological features of focal nodular hyperplasia in Gd-EOB-DTPA-enhanced liver magnetic resonance imaging: results of a multicenter trial. Investigative radiology. 2008; 43:504–511. [PubMed: 18580333]
4. Kwon HJ, Byun JH, Kim JY, et al. Differentiation of small (</=2 cm) hepatocellular carcinomas from small benign nodules in cirrhotic liver on gadoxetic acid-enhanced and diffusion-weighted magnetic resonance images. Abdominal imaging. 2014
5. Motosugi U, Ichikawa T, Sou H, et al. Distinguishing hypervascular pseudolesions of the liver from hypervascular hepatocellular carcinomas with gadoxetic acid-enhanced MR imaging. Radiology. 2010; 256:151–158. [PubMed: 20574092]
6. Park MJ, Kim YK, Lee MW, et al. Small hepatocellular carcinomas: improved sensitivity by combining gadoxetic acid-enhanced and diffusion-weighted MR imaging patterns. Radiology. 2012; 264:761–770. [PubMed: 22843769]
7. Phongkitkarun S, Limsamutpetch K, Tannaphai P, Jatchavala J. Added value of hepatobiliary phase gadoxetic acid-enhanced MRI for diagnosing hepatocellular carcinoma in high-risk patients. World journal of gastroenterology : WJG. 2013; 19:8357–8365. [PubMed: 24363528]
8. Yoneda N, Matsui O, Kitao A, et al. Hypervascular hepatocellular carcinomas showing hyperintensity on hepatobiliary phase of gadoxetic acid-enhanced magnetic resonance imaging: a possible subtype with mature hepatocyte nature. Japanese journal of radiology. 2013; 31:480–490. [PubMed: 23771695]
9. Choi JW, Lee JM, Kim SJ, et al. Hepatocellular carcinoma: imaging patterns on gadoxetic acid-enhanced MR Images and their value as an imaging biomarker. Radiology. 2013; 267:776–786. [PubMed: 23401584]
10. Choi YS, Rhee H, Choi JY, et al. Histological characteristics of small hepatocellular carcinomas showing atypical enhancement patterns on gadoxetic acid-enhanced MR imaging. Journal of magnetic resonance imaging : JMRI. 2013; 37:1384–1391. [PubMed: 23172629]
11. Golfieri R, Grazioli L, Orlando E, et al. Which is the best MRI marker of malignancy for atypical cirrhotic nodules: hypointensity in hepatobiliary phase alone or combined with other features? Classification after Gd-EOB-DTPA administration. Journal of magnetic resonance imaging : JMRI. 2012; 36:648–657. [PubMed: 22592930]
12. Nakamura S, Nakaura T, Kidoh M, et al. Timing of the hepatic arterial phase at Gd-EOB-DTPA-enhanced hepatic dynamic MRI: comparison of the test-injection and the fixed-time delay method. Journal of magnetic resonance imaging : JMRI. 2013; 38:548–554. [PubMed: 23744782]
13. Goshima S, Kanematsu M, Kondo H, et al. Evaluation of optimal scan delay for gadoxetate disodium-enhanced hepatic arterial phase MRI using MR fluoroscopic triggering and slow injection technique. AJR American journal of roentgenology. 2013; 201:578–582. [PubMed: 23971449]
14. Ito K, Fujita T, Shimizu A, et al. Multiarterial phase dynamic MRI of small early enhancing hepatic lesions in cirrhosis or chronic hepatitis: differentiating between hypervascular hepatocellular carcinomas and pseudolesions. AJR American journal of roentgenology. 2004; 183:699–705. [PubMed: 15333358]
15. Kumano S, Uemura M, Haraikawa T, et al. Efficacy of double arterial phase dynamic magnetic resonance imaging with the sensitivity encoding technique versus dynamic multidetector-row helical computed tomography for detecting hypervascular hepatocellular carcinoma. Japanese journal of radiology. 2009; 27:229–236. [PubMed: 19626408]
16. Low RN, Bayram E, Panchal NJ, Estkowski L. High-resolution double arterial phase hepatic MRI using adaptive 2D centric view ordering: initial clinical experience. AJR American journal of roentgenology. 2010; 194:947–956. [PubMed: 20308496]

17. Davenport MS, Caoili EM, Kaza RK, Hussain HK. Matched within-patient cohort study of transient arterial phase respiratory motion-related artifact in MR imaging of the liver: gadoxetate disodium versus gadobenate dimeglumine. Radiology. 2014; 272:123–131. [PubMed: 24617733]
18. Davenport MS, Viglianti BL, Al-Hawary MM, et al. Comparison of acute transient dyspnea after intravenous administration of gadoxetate disodium and gadobenate dimeglumine: effect on arterial phase image quality. Radiology. 2013; 266:452–461. [PubMed: 23192781]
19. Pietryga JA, Burke LM, Marin D, Jaffe TA, Bashir MR. Respiratory motion artifact affecting hepatic arterial phase imaging with gadoxetate disodium: examination recovery with a multiple arterial phase acquisition. Radiology. 2014; 271:426–434. [PubMed: 24475864]
20. Chandarana H, Feng L, Block TK, et al. Free-breathing contrast-enhanced multiphase MRI of the liver using a combination of compressed sensing, parallel imaging, and golden-angle radial sampling. Investigative radiology. 2013; 48:10–16. [PubMed: 23192165]
21. Feng L, Grimm R, Block KT, et al. Golden-angle radial sparse parallel MRI: Combination of compressed sensing, parallel imaging, and golden-angle radial sampling for fast and flexible dynamic volumetric MRI. Magn Reson Med. 2014; 72(3):707–717. [PubMed: 24142845]
22. Azevedo RM, de Campos RO, Ramalho M, Heredia V, Dale BM, Semelka RC. Free-breathing 3D T1-weighted gradient-echo sequence with radial data sampling in abdominal MRI: preliminary observations. AJR American journal of roentgenology. 2011; 197:650–657. [PubMed: 21862807]
23. Chandarana H, Block TK, Rosenkrantz AB, et al. Free-breathing radial 3D fat-suppressed T1-weighted gradient echo sequence: a viable alternative for contrast-enhanced liver imaging in patients unable to suspend respiration. Investigative radiology. 2011; 46:648–653. [PubMed: 21577119]
24. Winkelmann S, Schaeffter T, Koehler T, Eggers H, Doessel O. An optimal radial profile order based on the Golden Ratio for time-resolved MRI. IEEE transactions on medical imaging. 2007; 26:68–76. [PubMed: 17243585]
25. BLINDED.
26. Fessler JA, Sutton BP. Nonuniform Fast Fourier Transforms Using Min-Max Interpolation. IEEE Transactions on Signal Processing. 2003; 51:560–574.
27. Hamm B, Staks T, Muhler A, et al. Phase I clinical evaluation of Gd-EOB-DTPA as a hepatobiliary MR contrast agent: safety, pharmacokinetics, and MR imaging. Radiology. 1995; 195:785–792. [PubMed: 7754011]
28. Motosugi U, Ichikawa T, Sou H, et al. Liver parenchymal enhancement of hepatocyte-phase images in Gd-EOB-DTPA-enhanced MR imaging: which biological markers of the liver function affect the enhancement? Journal of magnetic resonance imaging : JMRI. 2009; 30:1042–1046. [PubMed: 19856436]
29. van Montfoort JE, Stieger B, Meijer DK, Weinmann HJ, Meier PJ, Fattinger KE. Hepatic uptake of the magnetic resonance imaging contrast agent gadoxetate by the organic anion transporting polypeptide Oatp1. The Journal of pharmacology and experimental therapeutics. 1999; 290:153–157. [PubMed: 10381771]
30. Tamada T, Ito K, Sone T, et al. Dynamic contrast-enhanced magnetic resonance imaging of abdominal solid organ and major vessel: comparison of enhancement effect between Gd-EOB-DTPA and Gd-DTPA. Journal of magnetic resonance imaging : JMRI. 2009; 29:636–640. [PubMed: 19243060]
31. Reiner CS, Neville AM, Nazeer HK, et al. Contrast-enhanced free-breathing 3D T1-weighted gradient-echo sequence for hepatobiliary MRI in patients with breath-holding difficulties. Eur Radiol. 2013; 23(11):3087–3093. [PubMed: 23732689]
32. Chandarana H, Block KT, Winfeld MJ, et al. Free-breathing contrast-enhanced T1-weighted gradient-echo imaging with radial k-space sampling for paediatric abdominopelvic MRI. European radiology. 2014; 24:320–326. [PubMed: 24220754]
33. Riffel P, Attenberger UI, Kannengiesser S, et al. Highly accelerated T1-weighted abdominal imaging using 2-dimensional controlled aliasing in parallel imaging results in higher acceleration: a comparison with generalized autocalibrating partially parallel acquisitions parallel imaging. Invest Radiol. 2013; 48(7):554–561. [PubMed: 23462674]

34. Kazmierczak PM, Theisen D, Thierfelder KM, et al. Improved detection of hypervascular liver lesions with CAIPIRINHA-Dixon-TWIST-volume-interpolated breath-hold examination. Invest Radiol. 2015; 50(3):153–160. [PubMed: 25478742]

35. Cheng, JYZT.; Pauly, JM.; Vasanawala, SS.; Lustig, M. Free Breathing Dynamic Contrast Enhanced 3D MRI with Resolved Respiratory Motion. Proceedings of the 22th Annual Meeting of ISMRM; Milan, Italy. 2014. p. 330

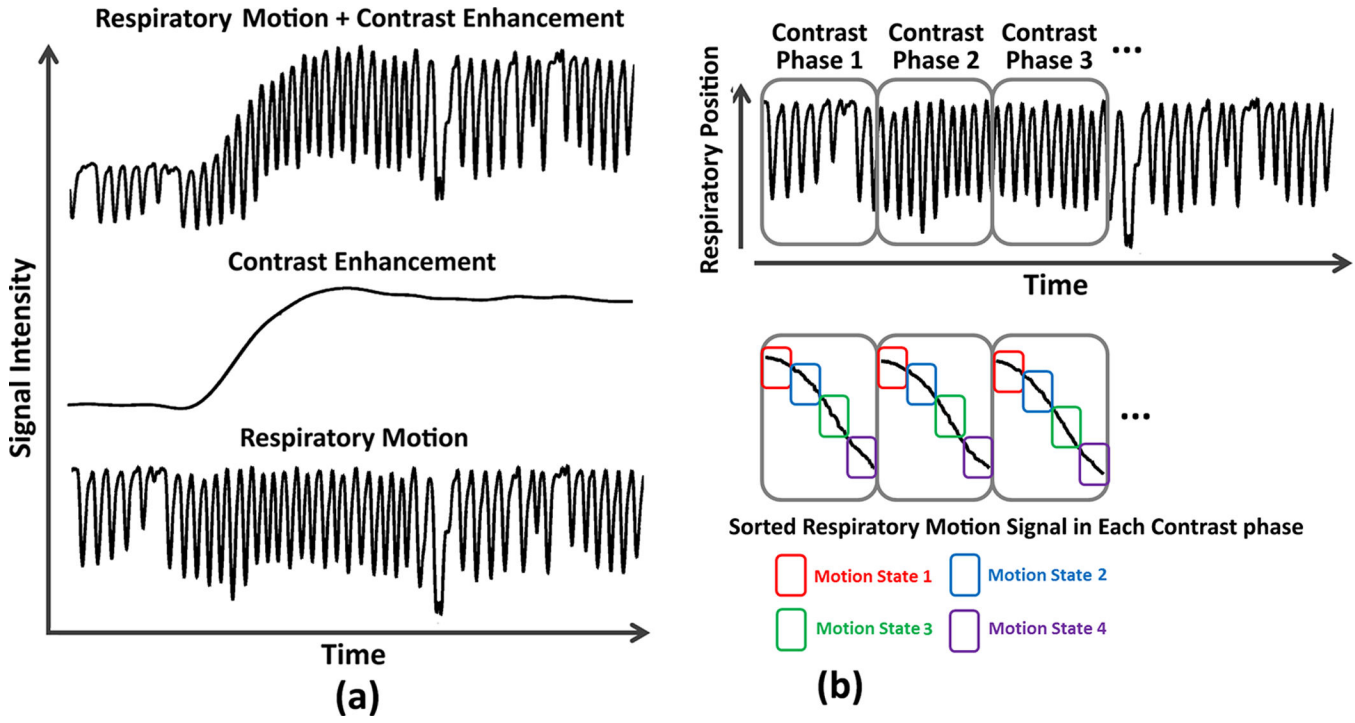

Figure 1.

Schematic of the sorting of the continuously acquired radial spokes in to different phases of contrast enhancement and in 4 respiratory motion states. The motion sorted undersampled data for each phase of enhancement was reconstructed with XD-GRASP technique. XD-GRASP reconstructions in end-expiratory phase (motion state 1) of the respiratory cycle were used for image analysis and quality comparison.

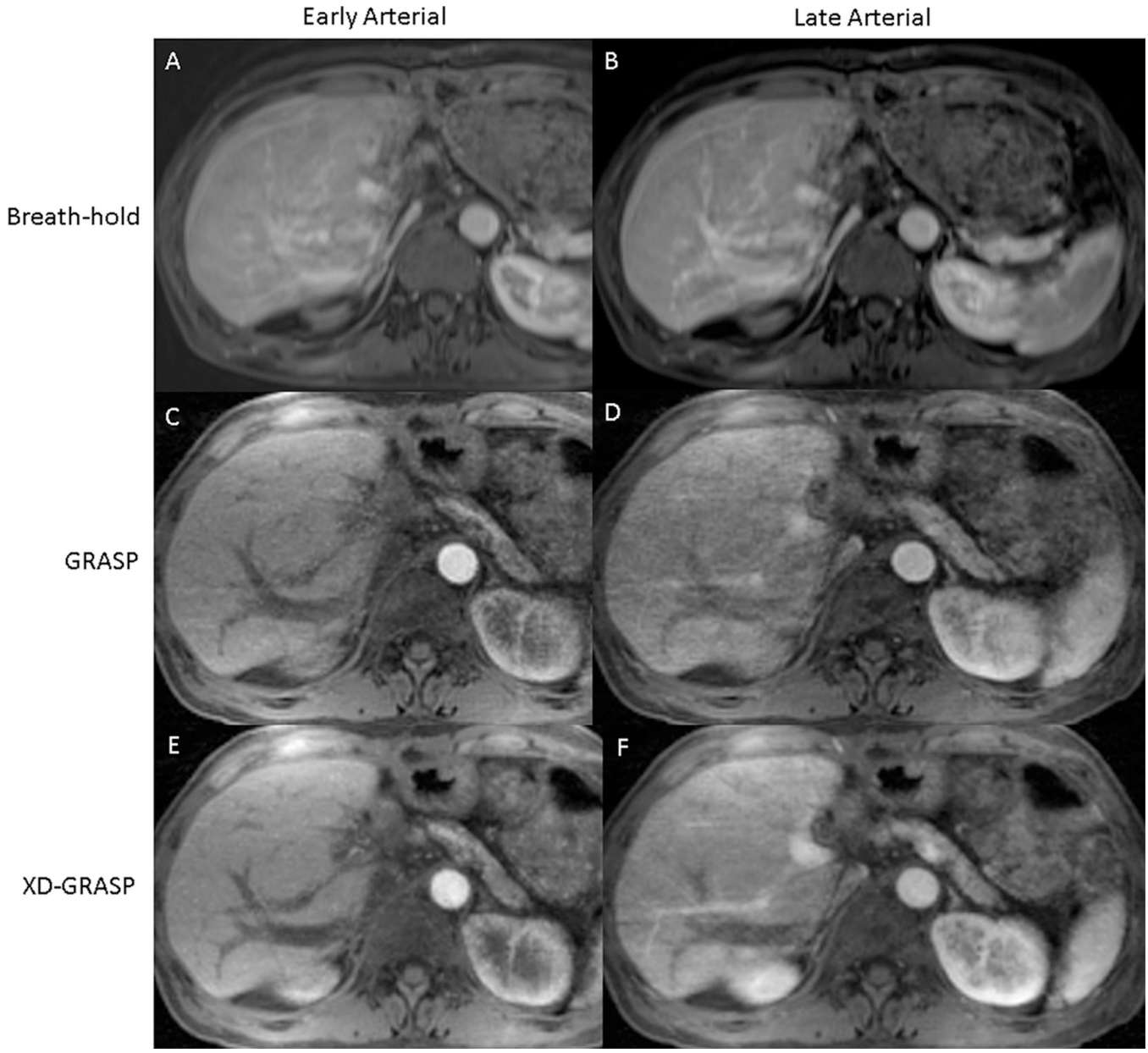

Figure 2.

Comparison of prior breath-hold Cartesian (A & B), free-breathing GRASP (C & D), and free-breathing XD-GRASP (E & F) studies in a 40 year old female patient undergoing post-liver-transplant surveillance. The left column shows early-arterial-phase acquisitions, and the right column shows late-arterial-phase acquisitions. For the Cartesian study, both early (A) and late (B) arterial phase acquisitions were performed in a single breath-hold. A subsequent exam was performed in the same patient with free-breathing radial acquisition during contrast injection. Early and late phase arterial phases of enhancement were reconstructed from the same raw data using GRASP (C & D) and XD-GRASP (E & F). XD-GRASP reconstructions received higher scores of image quality from both readers compared to GRASP and BH exam.

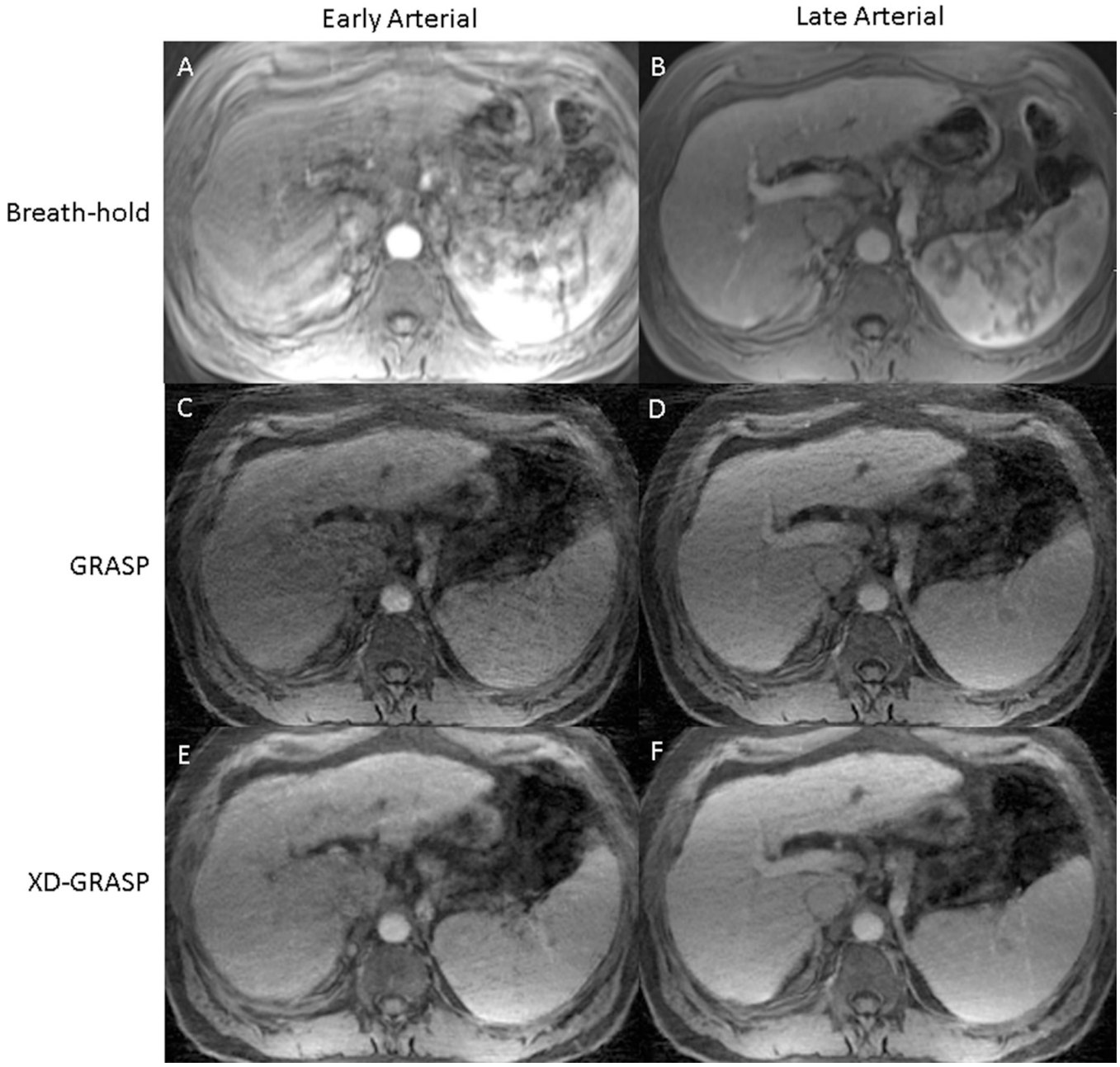

Figure 3.

Comparison of prior breath-hold Cartesian (A & B), free-breathing GRASP (C & D), and free-breathing XD-GRASP (E & F) arterial phases in a cirrhotic patient. XD-GRASP images received the highest score for overall image quality from both readers.

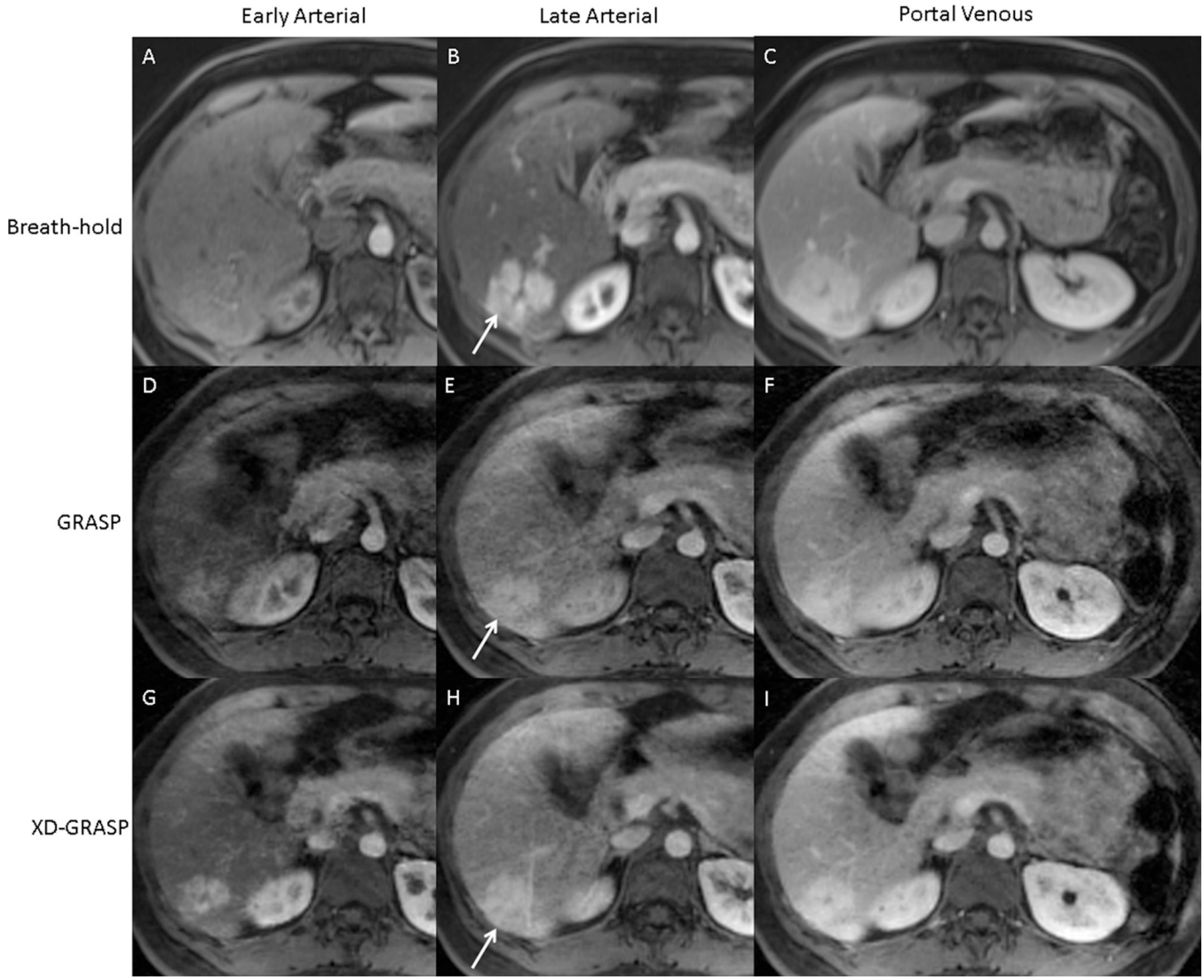

Figure 4.

Comparison of images obtained in a 56 year old female with known diagnosis of FNH (arrow) in early arterial, late arterial, and portal venous phases of contrast enhancement with a prior breath-held post-contrast acquisition (A, B, C), as well as with GRASP (D, E, F) and XD-GRASP (G, H, I) reconstruction of a subsequent free-breathing continuous radial acquisition.

Table 1

Scoring for various parameters of image quality for each acquisition/reconstruction scheme and for each phase of enhancement

Image quality Parameter	Score	Scoring system
Overall Image Quality	1 – 5	1. Unacceptable; 2. Poor; 3. Acceptable; 4. Good; 5. Excellent
Liver Edge Sharpness & Hepatic Vessel Clarity	1 – 5	1. Unreadable; 2. Extreme blur; 3. Moderate blur; 4. Mild blur; 5. No blur
Streak Artifact	1 – 5	1. Unreadable; 2. Extreme artifact; 3. Moderate artifact; 4. Mild artifact; 5. No artifact
Lesion Conspicuity	1 – 5	1. Unreadable; 2. Poor; 3. Acceptable; 4. Good; 5. Excellent
Lesion Edge Sharpness	1 – 5	1. Unreadable; 2. Extreme blur; 3. Moderate blur; 4. Mild blur; 5. No blur

Table 2

A: Overall image quality scores provided by two readers for each phase of enhancement and for each acquisition/reconstruction scheme. Scores in early and late arterial phases are highlighted in bold.						
Overall Image Quality	**GRASP**		**XD-GRASP**		**BH VIBE**	
Phase of Enhancement	**Reader 1**	**Reader 2**	**Reader 1**	**Reader 2**	**Reader 1**	**Reader 2**
Non-contrast	3.50 ± 0.6	3.75 ± 1.1	3.94 ± 0.4	4.1 ± 0.8	3.94 ± 0.6	4.13 ± 0.6
Early Arterial	**3.31 ± 0.6**	**3.38 ± 0.9**	**4.3 ± 0.6**	**3.81 ± 0.8**	**3.88 ± 0.6**	**3.50 ± 1.0**
Late Arterial	**3.63 ± 0.6**	**2.88 ± 0.7**	**4.5 ± 0.6**	**3.56 ± 0.5**	**3.44 ± 0.6**	**2.94 ± 0.9**
Portal Venous	3.75 ± 0.8	3.81 ± 0.9	4.44 ± 0.5	4.0 ± 0.5	4.38 ± 0.6	4.0 ± 0.7

B: P value for pair-wise comparison of overall image quality score between acquisitions for each phase of enhancement stratified by reader. Significant differences are highlighted in bold.					
Comparison	**Reader**	**Non-contrast**	**Early Arterial**	**Late Arterial**	**Portal Venous**
XD-GRASP versus GRASP	1	0.063	**<0.001**	**0.001**	**0.002**
XD-GRASP versus GRASP	2	**0.031**	**0.016**	**0.002**	0.508
XD-GRASP versus BH VIBE	1	1.000	0.183	**0.001**	1.000
XD-GRASP versus BH VIBE	2	1.000	0.391	**0.039**	1.000

Table 3

A: Scores for hepatic vessel clarity provided by two readers for each phases of enhancement. Scores in early and late arterial phases are highlighted in bold.						
Hepatic Vessel Clarity	**GRASP**		**XD-GRASP**		**BH VIBE**	
Phase of Enhancement	**Reader 1**	**Reader 2**	**Reader 1**	**Reader 2**	**Reader 1**	**Reader 2**
Non-contrast	3.25 ± 0.8	3.81 ± 1.2	3.69 ± 0.8	3.94 ± 1.1	3.44 ± 0.6	4.19 ± 0.8
Early Arterial	**3.38 ± 0.6**	**3.44 ± 1.3**	**4.0 ± 0.7**	**3.81 ± 1.1**	**3.63 ± 0.8**	**3.88 ± 0.9**
Late Arterial	**3.50 ± 0.7**	**3.00 ± 1.0**	**4.19 ± 0.7**	**3.44 ± 1.0**	**3.56 ± 0.7**	**3.31 ± 1.1**
Portal Venous	3.69 ± 0.9	3.81 ± 0.9	4.19 ± 0.7	3.75 ± 0.9	4.31 ± 0.6	4.06 ± 0.8

B: P value for pair-wise comparison of hepatic vessel clarity score between acquisitions for each phase of enhancement stratified by reader. Significant differences are highlighted in bold.					
Comparison	**Reader**	**Non-contrast**	**Early Arterial**	**Late Arterial**	**Portal Venous**
XD-GRASP versus GRASP	1	0.121	**0.004**	**0.002**	**0.008**
XD-GRASP versus GRASP	2	0.625	0.063	0.063	1.000
XD-GRASP versus BH VIBE	1	0.344	0.183	**0.043**	0.781
XD-GRASP versus BH VIBE	2	0.398	0.773	1.000	0.363

Table 4

A: Scores for liver edge sharpness provided by two readers for each phases of enhancement. Scores in early and late arterial phases are highlighted in bold.						
Liver Edge Sharpness	**GRASP**		**XD-GRASP**		**BH VIBE**	
Phase of Enhancement	**Reader 1**	**Reader 2**	**Reader 1**	**Reader 2**	**Reader 1**	**Reader 2**
Non-contrast	3.81 ± 0.8	4.13± 0.7	4.13 ± 0.5	4.31 ± 0.7	4.25 ± 0.6	4.31 ± 0.6
Early Arterial	**3.81 ± 0.8**	**3.88 ± 0.7**	**4.31 ± 0.6**	**4.19 ± 0.8**	**3.94 ± 0.7**	**3.81 ± 1.1**
Late Arterial	**3.75 ± 0.7**	**3.50 ± 0.6**	**4.38 ± 0.7**	**3.69 ± 1.0**	**3.38 ± 0.7**	**3.13 ± 1.1**
Portal Venous	3.81 ± 0.8	4.19 ± 0.7	4.31 ± 0.7	4.06 ± 0.8	4.44 ± 0.5	4.25 ± 0.5

B: P value for pair-wise comparison of hepatic vessel clarity score between acquisitions for each phase of enhancement stratified by reader. Significant differences are highlighted in bold.					
Comparison	**Reader**	**Non-contrast**	**Early Arterial**	**Late Arterial**	**Portal Venous**
XD-GRASP versus GRASP	1	0.125	**0.008**	**0.002**	**0.016**
XD-GRASP versus GRASP	2	0.531	0.063	0.563	0.781
XD-GRASP versus BH VIBE	1	0.688	0.172	**0.001**	0.727
XD-GRASP versus BH VIBE	2	1.000	0.236	0.107	0.563

Table 5

Scores for streak artifact as assessed by two readers for each phases of enhancement for GRASP and XD-GRASP reconstructions. In all cases, XD-GRASP had lower radial spokes related artifacts and hence higher scores which was significant for reader 1 (all $p < 0.05$) but not for reader 2.

Streak Artifact	**GRASP**		**XD-GRASP**	
Phase of Enhancement	**Reader 1**	**Reader 2**	**Reader 1**	**Reader 2**
Non-contrast	3.31 ± 0.6	3.81 ± 0.8	3.94 ± 0.6	4.00 ± 0.7
Early Arterial	3.25 ± 0.7	3.56 ± 0.8	4.06 ± 0.6	3.81 ± 0.8
Late Arterial	3.31 ± 0.6	3.38 ± 0.6	4.06 ± 0.6	3.54 ± 0.6
Portal Venous	3.44 ± 0.6	3.81 ± 0.7	3.94 ± 0.4	3.94 ± 0.6